PHYSICAL REVIEW B **90**, 180407(R) (2014)

Testing spin-flip scattering as a possible mechanism of ultrafast demagnetization in ordered magnetic alloys

Stefan Günther,[1] Carlo Spezzani,[2] Roberta Ciprian,[3] Cesare Grazioli,[2,4] Barbara Ressel,[4] Marcello Coreno,[2,5] Luca Poletto,[6] Paolo Miotti,[6] Maurizio Sacchi,[7,8,9] Giancarlo Panaccione,[3] Vojtěch Uhlíř,[10] Eric E. Fullerton,[10] Giovanni De Ninno,[4,2] and Christian H. Back[1]

[1]*University of Regensburg, Regensburg, Germany*
[2]*Elettra Sincrotrone Trieste, Trieste, Italy*
[3]*Istituto Officina dei Materiali (IOM)-CNR, Laboratorio TASC, Area Science Park, S.S.14, Km 163.5, I-34149 Trieste, Italy*
[4]*Laboratory of Quantum Optics, University of Nova Gorica, Nova Gorica, Slovenia*
[5]*Institute of Inorganic Methodologies and Plasmas (CNR-IMIP), Montelibretti, Rome, Italy*
[6]*Institute of Photonics and Nanotechnologies (CNR-IFN), Padova, Italy*
[7]*Sorbonne Universités, UPMC Univ Paris 06, UMR 7588, INSP, F-75005, Paris, France*
[8]*CNRS, UMR 7588, Institut des NanoSciences de Paris, F-75005, Paris, France*
[9]*Synchrotron SOLEIL, L'Orme des Merisiers, Saint-Aubin, France*
[10]*Center for Magnetic Recording Research, University of California, San Diego, La Jolla, California 92093-0401, USA*

(Received 10 April 2014; revised manuscript received 31 October 2014; published 21 November 2014)

We use element-resolved IR-pump/extreme ultraviolet-probe experiments to disentangle the ultrafast interplay of the magnetic sublattices of an ordered crystalline magnetic alloy. As a paradigmatic example, we investigate the case of the FeRh alloy, which shows a delayed response for the different components. Furthermore, a detailed time-resolved magneto-optic study shows that the data can be analyzed by only assuming Elliot-Yafet-like scattering, as the underlying mechanism for ultrafast demagnetization, resulting in an unexpected nonmonotonic dependence of the spin-flip rate, as a function of quenching.

DOI: 10.1103/PhysRevB.90.180407 PACS number(s): 75.78.Jp

In recent years a substantial experimental effort has been devoted to the study of ultrafast demagnetization and all-optical switching of ferro- and ferrimagnetic alloys. Understanding these phenomena is of interest for heat assisted magnetic recording and all-optical magnetic recording [1]; however, unraveling the microscopic mechanisms behind the observed dynamic response has remained a formidable task. Several theories have been put forward, claiming to be able to explain ultrafast demagnetization in general [2–9] and in particular the response of multisublattice systems where two or more magnetic elements form a ferro- or ferrimagnetically coupled ordered system [10–12]. In these systems, a crucial question is how different elements in an alloy interact on a ultrashort time scale close to the time scale corresponding to the exchange interaction (10–100 fs).

Element-specific probes [13–15] as well as systematic studies using more conventional time-resolved techniques [16] on ultrashort time scales have contributed greatly in the advancement of knowledge in this particular field. For example, for ferrimagnetic $3d$ transition metal/$4f$ rare earth alloys ($3d$-$4f$) such as CoFeGd that are used for all-optical switching, a transient ferromagnetic state exists in the process of ultrafast magnetization reversal [17]. In spite of their strong antiferromagnetic exchange coupling, the individual components of these systems show independent demagnetization dynamics characterized by different demagnetization times. Furthermore, it has been shown recently that highly ordered $3d$-$4f$ multilayer systems can also be used for all-optical switching [18].

Theoretical models based on a description of different anti- or ferromagnetically coupled sublattices with distinct coupling constants have been put forward to explain the element-specific behavior of these systems [10–12]. However, a consensus on the underlying microscopic demagnetization process in multisublattice systems is still lacking.

Interestingly, there seems to be no experimental consensus on the demagnetization dynamics even for ferromagnetically coupled multisublattice systems such as simple $3d$ transition metal alloys. In the case of NiFe, for instance, two different element-specific experimental probes performed at the $2p$ and $3p$ resonances (time-resolved magneto-optics at the L or M edges) gave contrasting results, with Ni demagnetizing either faster [19] or slower [20] than Fe. There is thus the need to study and unravel the demagnetization behavior of multisublattice systems in particular, in view of understanding the possibly technologically relevant all-optical switching mechanism. One experimental shortcoming that complicates a direct comparison to theoretical predictions (in particular, predictions based on the electronic band structure [21]) is the fact that so far only disordered or polycrystalline alloys have been studied experimentally. Concentrating on theoretically more easily accessible ordered crystalline alloys can help to understand the origin of the different demagnetization dynamics of the alloy components, by comparing experiments to theoretical calculations. In this Rapid Communication, we concentrate on an ordered multisublattice system, the ordered alloy FeRh, a single-crystalline material with a well-known electronic band structure [22]. This ordered alloy undergoes a first-order phase transition from an antiferromagnetically ordered phase to a ferromagnetically ordered phase at temperatures slightly above room temperature. The second-order phase transition to the paramagnetic phase occurs around 660 K. Quite a few time-resolved experiments have addressed the fundamental question of the ultimate time scale for the generation of magnetic order in this particular system when driven through the first-order phase transition. However, only little is known about the demagnetization dynamics of the FeRh system when excited by powerful laser pulses in its ferromagnetic state [23], which is at the heart of this

Rapid Communication. Two experimental methods based on time-resolved magneto-optics are exploited. We use the time-resolved magneto-optic Kerr effect (TR-MOKE) in the visible to IR range as well as in the extreme ultraviolet (XUV) (TR-XUV-MOKE) domain. Using high harmonic generation (HHG), element-specific information can be accessed at the *M*/*N* edges. Our element-specific experiments indicate that the demagnetization of Fe is delayed with respect to Rh, and it has a slightly shorter demagnetization time. This finding is supported by the microscopic three-temperature model (M3TM) [2] which we employ to model our data. Additional detailed TR-MOKE experiments, presented in the following, allow us to test the M3TM model more accurately and reveal a clear dependence of the spin-flip rate on the exciting laser fluence, which cannot be accounted for within a rigid band approach, where the spin-flip rate stays constant.

For the experiments we use epitaxially grown FeRh films with a thickness of 50 nm deposited onto a MgO(001) substrate by magnetron sputtering from a single equiatomic target. The FeRh films grow epitaxially with (001) orientation. The high quality films show a typical temperature hysteresis of 20 K with the first-order phase transition from the antiferromagnetic to the ferromagnetic phase appearing around 360 K. The Curie temperature is reached at 660 K.

In order to study the element selective ultrafast demagnetization dynamics of FeRh, we have implemented a TR-XUV-MOKE experiment at the HHG beamline CITIUS [24] (see Fig. 1). This light source is based on standard HHG in noble gases [25,26] and makes use of a high power Ti:sapphire ultrashort laser amplifier delivering 3 mJ pulses at 800 nm (repetition rate 5 kHz) with a typical pulse duration of 35 fs [24]. A beam splitter is used to supply HHG with two thirds

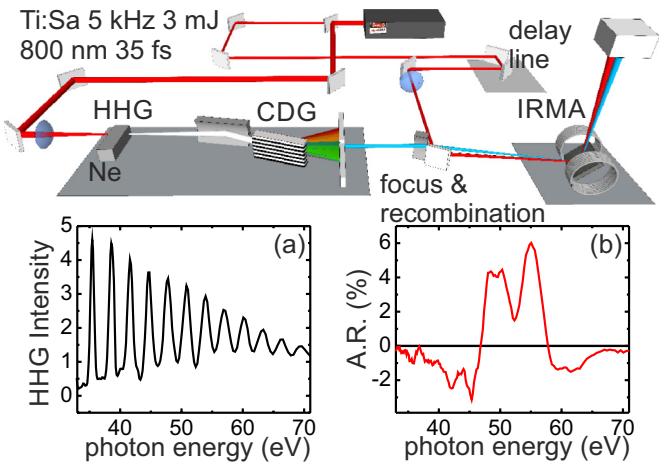

FIG. 1. (Color online) Sketch of the CITIUS HHG light source. The 3 mJ/pulse Ti:sapphire laser output is split in two branches: 2 mJ/pulse is used for HHG and 1 mJ/pulse for sample excitation (IR pump). The proper harmonic is selected by means of a time preserving monochromator based on conical diffraction gratings (CDGs) and refocalized onto the sample. The IR pump is recombined with the HHG light in the experimental chamber IRMA on the sample in an almost collinear geometry. (a) The higher harmonics spectrum from Ne after the monochromator captured with a photodiode and (b) the normalized magnetic asymmetry ratio (A.R.), namely, the difference of both field directions divided by their sum, for the T-MOKE-like configuration in the IRMA setup.

of the amplifier output. The remaining fraction is used for the excitation of the system using a variable time delay. High harmonics up to order (H)51 of the fundamental wavelength with a linear vertical polarization are obtained.

A spectral selection of the light sent to the sample is made by means of a pulse-duration preserving monochromator [27,28]. The IR pump [spot size about 500 μm full width at half maximum (FWHM)] and XUV probe beam (spot size about 200 μm FWHM) are recombined on the sample in an almost collinear geometry in the IRMA reflectometer, featuring a vertical scattering plane [29]. The maximum temporal inaccuracy by changing the XUV wavelength, due to movements in the monochromator, is estimated to be below 5 fs for the chosen harmonics. A detailed technical description of the HHG beamline can be found in Ref. [24]. The scattered light is detected using a photodiode mounted on the detector arm, shielded with a 200 nm thick Al filter to block the IR pump. In the T-MOKE-like configuration using *p*-polarized XUV light, one is sensitive to the magnetization component perpendicular to the scattering plane. Choosing the incoming/scattering angle close to the Brewster condition (about 45° at 54 eV), the magnetization contrast is maximized with respect to the strongly suppressed nonmagnetic scattered background [30,31]. By varying the photon energy, the harmonics for the Fe *M* (H35, i.e., 54 eV) and Rh *N* edges (H31/H33, i.e., 48/51 eV) can be identified and the signals of the two chosen harmonics (H31 and H35) are clearly separated [see Fig. 1(b)]. To avoid long-term drifts, the magnetic asymmetry for Fe and Rh is measured via field reversal at every time delay between the IR pump and XUV probe, and then multiple demagnetization traces are averaged. In the following, t_0 is defined as the average value for the beginning of the initial drop of the magnetization of Fe and Rh.

In addition, two color TR-MOKE experiments are performed. For these measurements we use a regenerative amplified Ti:sapphire laser, which provides up to 4 μJ pulses with a pulse length below 50 fs and a repetition rate which is adjustable between 70 and 250 kHz. We use the fundamental IR pulse (800 nm) for pumping and the second harmonic visible pulse (400 nm) for probing the magnetic state. The temperature is kept constant at 400 K for all measurements.

Two typical TR-XUV-MOKE demagnetization traces in the fully ferromagnetic phase (which is verified by recording a static temperature hysteresis loop) are plotted for two different fluences in Figs. 2(a) and 2(b). The fit (solid line) is performed using the M3TM with initial parameters obtained by TR-MOKE on the same sample, which will be further addressed below. A small but non-negligible shift in time zero of the two different element-specific demagnetization traces appears within experimental accuracy in all measurements. We find that Fe is delayed with respect to Rh by approximately 60 fs, and the evolution of the shift as a function of pump fluence (or respective quenching) is summarized in Fig. 4(c). Moreover, we find that the demagnetization time of Fe is slightly shorter (by about 25 fs) than that of Rh. We would like to note that the time shift between Fe and Rh is confirmed by a fully statistical analysis of the data, see Supplemental Material [32].

To shed further light on the experimental findings and to test the validity of the use of the M3TM, we perform

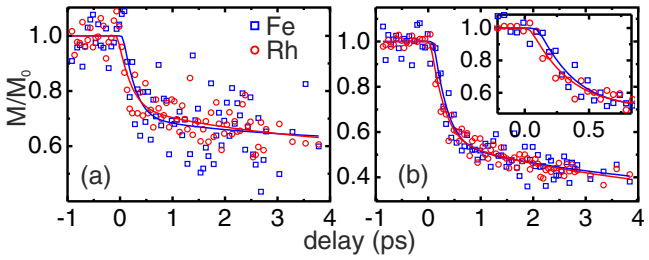

FIG. 2. (Color online) Element-resolved demagnetization dynamics of FeRh (Fe: blue open squares; Rh: red open circles) obtained by TR-XUV-TMOKE. The reduced magnetization (M/M_0) after excitation with (a) 11 mJ/cm^2 and (b) 16 mJ/cm^2. The inset in (b) shows a zoom to the initial drop of the signal. Fe demagnetization is delayed with respect to Rh by approximately 60 fs.

detailed TR-MOKE experiments at lower pump fluences with a higher signal-to-noise ratio with respect to XUV-MOKE. We observe partial demagnetization of the FeRh films with an initial fast drop of the magnetization, followed by a decay with a much lower rate before the system starts to relax back to its equilibrium value (see Fig. 3), which—in the classification of Koopmans *et al.* [2]—is called type II demagnetization behavior with a transition to type I (no slow decay) for the lowest fluence. When increasing the incident fluence, the quenching ($1 - M/M_0$) increases and the type II behavior becomes more pronounced.

Since for type II behavior the definition of the time scale for the initial fast drop of the magnetization is somewhat arbitrary, in this Rapid Communication the demagnetization time for type II demagnetization is defined as the time where the system has completed $1/e$ of its demagnetization with respect to its value at 1 ps after time zero t_0. The quenching is consequently defined as the value at 1 ps (see Fig. 3).

In the following we will relate our findings to existing models for demagnetization in multisublattice systems [10,12]. Not all existing models can be applied to our experimental system since the typical input parameters for these models are related to the "pure" phase, in our case pure Fe or pure Rh. Even though the magnetic moments of Fe and Rh in the ferromagnetic phase are known [33,34], the moment of Rh in the pure phase vanishes and consequently a demagnetization

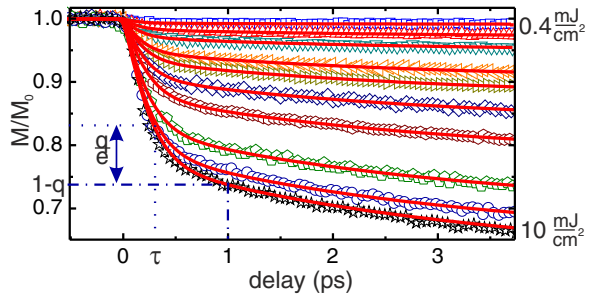

FIG. 3. (Color online) TR-MOKE demagnetization traces of FeRh for various fluences (0.4–10 mJ/cm^2). The solid line (red) is a fit using the M3TM model, where only the spin-flip rate and the excitation strength is allowed to vary. The demagnetization time τ (dotted line) referenced to the quenching q (defined as the loss of magnetization at 1 ps, dashed-dotted line) is visualized for the trace with the highest fluence (10 mJ/cm^2).

time cannot be determined. In systems where a "pure" phase exists, such as in Fe-Ni alloys, it was shown that the difference in t_0 and τ is related to the strength of the exchange coupling between the involved sublattices [20].

Note that the experimentally observed shift in t_0 can be explained by using Elliot-Yafet-type spin-flip scattering as a key mechanism, and therefore our data can be analyzed within the M3TM model [2,12]. We would like to note that other theories relying on Elliot-Yafet-type spin-flip scattering (with and without a dynamic feedback mechanism) [21,35] may be able to explain the data as well. In our case we stick to the simple M3TM model in a rigid-band-like approach which, in principle, can be applied without the need for band structure calculations. It is exactly the rigid band approach that will be under scrutiny in the following. We would also like to note that we neglect superdiffusive transport, which is probably an additional source for the loss of magnetic contrast [4], but is not discussed here, because it is a thin single-domain film deposited on an insulator.

The rate equations of the M3TM read

$$C_e[T_e]\frac{dT_e}{dt} = g_{ep}(T_p - T_e) + G(t_0, T_{e,\max}), \tag{1}$$

$$C_p\frac{dT_p}{dt} = g_{ep}(T_e - T_p). \tag{2}$$

$$\frac{dm}{dt} = R[g_{ep}, a_{sf}]m\frac{T_p}{T_C}\left[1 - m\coth\left(\frac{mT_c}{T_e}\right)\right], \tag{3}$$

where T_e and T_p denote the electronic and the phononic temperatures, $G(t_0, T_{e,\max})$ the Gaussian excitation due to the pump pulse at time zero (t_0) with a maximum electronic temperature $T_{e,\max}$, $m = \frac{M}{M_S}$ the magnetization relative to its expected zero temperature value, T_C the Curie temperature, g_{ep} the electron-phonon coupling, and C_p and C_e the specific heat of the phononic system and the electronic system (in linear approximation proportional to T_e with a proportionality constant γ). C_p is treated as a constant value for the entire covered temperature range, in agreement with static measurements [36]. $R = (8a_{\mathrm{sf}}g_{ep}k_BT_C^2)V_{\mathrm{at}}/(\frac{\mu_{\mathrm{at}}}{\mu_B}E_D^2)$ is a material-specific parameter, where $\frac{\mu_{\mathrm{at}}}{\mu_B}$ is the ratio of the atomic magnetic moment and the Bohr magnetron, V_{at} the atomic volume, E_D the Debye energy, and a_{sf} the spin-flip parameter, which is typically assumed to be constant within a rigid band approach. A cooling mechanism by heat diffusion to the substrate was found to be negligible for the behavior during the first 4 ps and is therefore neglected.

To obtain values for those variables that cannot be determined from static experiments, but are necessary to model the dynamic data (e.g., a_{sf}, γ, g_{ep}), the transient optical response for all fluences is fitted by Eqs. (1) and (2). With the assumption that the optical response is a good approximation for the electronic temperature, the electron specific heat shows a linear dependence and thus validates $C_e = \gamma T_e$. By additionally assuming $T_p \ll T_e$, g_{ep} can be determined on short time scales. Note that g_{ep} and a_{sf} can in principle be calculated using *ab initio* methods, at least in the limit $T_e \to 0$.

When fitting the traces for all fluences, it is possible to keep only three modeling parameters free, namely, the a_{sf}, $T_{e,\max}$, and t_0. Before fitting the experimental data with the Levenberg-Marquardt algorithm, the solution for M/M_0 of the

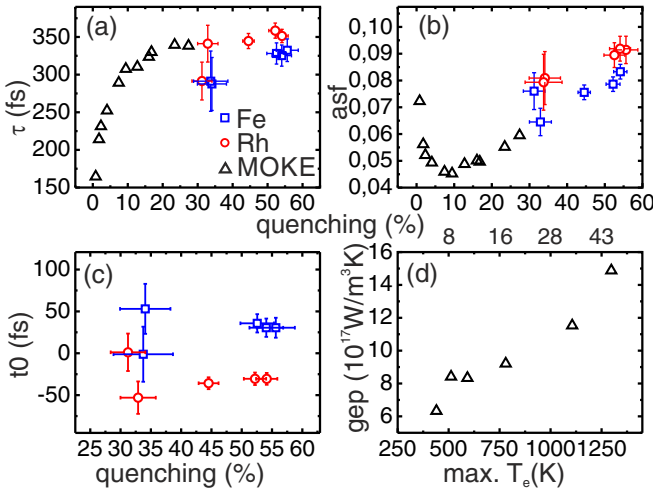

FIG. 4. (Color online) Fit parameters from the M3TM for element-resolved measurements, Rh (red open circles), Fe (blue open squares), and for TR-MOKE and the transient optical response (black open triangles; error bars are within the symbol size). (a) The demagnetization time τ and (b) the spin-flip rate a_{sf}, which is a key parameter for describing the demagnetization time and the quenching vs fluence. (c) The difference in t_0 for the element-resolved demagnetization times shows that Fe starts delayed by about 60 fs with respect to Rh for various fluences. Error bars for the lower fluence appear bigger due to a lower signal and a nearly constant noise level in all measurements. (d) The electron-phonon coupling g_{ep} is not constant as a function of the maximum electronic temperature or the resulting calculated quenching.

M3TM model is convoluted with a Gaussian pulse to account for the influence of the finite pulse length and the shape of the probing pulse.

Allowing only the spin-flip rate to vary—which strongly influences the demagnetization time and the quenching—the variation in the demagnetization time is also reflected by a drastic change in the spin-flip rate a_{sf} [Figs. 4(a) and 4(b)]. The demagnetization time τ shows a drastic change for low fluences while for intermediate and high fluences only small variations are observed. In the low fluence range the fast increase of the demagnetization time is caused by the steep decrease of the spin-flip rate a_{sf}. The nonlinear behavior of a_{sf} extracted from the M3TM is a clear indication that the electronic band structure changes and cannot be treated as being rigid with increasing fluence [37], however, the trend and the clearly visible minimum around 10% quenching still remain unclear.

We believe that the nonmonotonic behavior of a_{sf} is a clear indication of the oversimplification within the M3TM (use of rigid bands). We would also like to emphasize that the subtle effects observed here might disappear when polycrystalline or amorphous materials are investigated as opposed to the single-crystalline material studied here due to the loss of a well-defined electronic band structure. However, even for a single-crystalline material, detailed investigations of the dynamic band structure on short time scales are a formidable task and beyond the scope of this Rapid Communication. Nevertheless, the value for the spin-flip rate is always in the range of calculated values [22] for the spin-mixing parameter $\langle b^2 \rangle$, with $a_{sf} = p\langle b^2 \rangle$ and p ranging from 1.8 to 4. Furthermore, $\langle b^2 \rangle$ is calculated to be smaller on the Fe site than on the Rh site, which is also qualitatively reflected in the element-selective measurements [Fig. 4(b)]. Note that it is not possible to fit the fluence dependence by only varying the excitation energy. Although g_{ep} is expected not to change much in this fluence regime [38–40], the fit of the optical response reveals a different behavior [Fig. 4(d)], and may be related to changes of a_{sf} in the fit since a_{sf} and g_{ep} are somehow entangled. Fortunately, variations of g_{ep} are found to hardly influence the signature of a_{sf}, either with g_{ep} as a fitting parameter or with fixed values for each fluence, as indicated by carefully analyzing the transient optical response [Fig. 4(d)].

In summary, we have presented a fluence-dependent demagnetization experiment for an ordered single-crystalline alloy, with elemental resolution and additional information obtained by TR-MOKE. The data can be modeled using Elliot-Yafet-like scattering as a driving mechanism for ultrafast demagnetization within the framework of the M3TM. Furthermore, the observed element-dependent shift in t_0 can be qualitatively described within this theory. The strong hybridization between the Fe and Rh states results in a strong coupling of the Fe and Rh moments [22] and may therefore explain the relatively small differences between the demagnetization traces, in contrast to the larger differences observed in the much weaker coupled 3*d* transition metal rare earth alloys [17]. However, the observed dependence of the spin-flip rate a_{sf} with a clear visible minimum as a function of quenching (or fluence) cannot be understood within a rigid band approach and remains an unsolved problem awaiting further theoretical input. We would like to note here that this dependence can only be observed when a detailed set of experimental data as the one presented here is available. Moreover, it would be interesting to test in future calculations if, e.g., the proposed dynamic feedback mechanism within an Elliot-Yafet-like scattering approach [21] allows one to explain the data, or if the theory has to be refined even further. We would like to emphasize that the spin-flip rate should be accessible for single-crystalline ordered alloys from *ab initio* theories. A possible contribution from superdiffusive transport should also be present, but has not been treated here since the emphasis has been put on the explanation of the distinct demagnetization behavior of the two sublattices.

We would like to acknowledge Hubert Ebert for fruitful discussions. UCSD was supported under DOE-BES Award No. DE-SC0003678. The CITIUS project is funded by the program for crossborder cooperation between Italy and Slovenia 2007–2013.

[1] B. C. Stipe, T. C. Strand, C. C. Poon, H. Balamane, T. D. Boone, J. A. Katine, J.-L. Li, V. Rawat, H. Nemoto, A. Hirotsune *et al.*, Nat. Photonics **4**, 484 (2010).

[2] B. Koopmans, G. Malinowski, F. Dalla Longa, D. Steiauf, M. Fähnle, T. Roth, M. Cinchetti, and M. Aeschlimann, Nat. Mater. **9**, 259 (2010).

[3] M. Krauß, T. Roth, S. Alebrand, D. Steil, M. Cinchetti, M. Aeschlimann, and H. C. Schneider, Phys. Rev. B **80**, 180407 (2009).
[4] M. Battiato, K. Carva, and P. M. Oppeneer, Phys. Rev. Lett. **105**, 027203 (2010).
[5] M. Fähnle, M. Haag, and C. Illg, J. Magn. Magn. Mater. **347**, 45 (2013).
[6] E. Carpene, E. Mancini, C. Dallera, M. Brenna, E. Puppin, and S. De Silvestri, Phys. Rev. B **78**, 174422 (2008).
[7] G. P. Zhang and W. Hübner, Phys. Rev. Lett. **85**, 3025 (2000).
[8] B. Koopmans, J. J. M. Ruigrok, F. Dalla Longa, and W. J. M. de Jonge, Phys. Rev. Lett. **95**, 267207 (2005).
[9] J.-Y. Bigot, M. Vomir, and E. Beaurepaire, Nat. Phys. **5**, 515 (2009).
[10] J. H. Mentink, J. Hellsvik, D. V. Afanasiev, B. A. Ivanov, A. Kirilyuk, A. V. Kimel, O. Eriksson, M. I. Katsnelson, and T. Rasing, Phys. Rev. Lett. **108**, 057202 (2012).
[11] V. López-Flores, N. Bergeard, V. Halté, C. Stamm, N. Pontius, M. Hehn, E. Otero, E. Beaurepaire, and C. Boeglin, Phys. Rev. B **87**, 214412 (2013).
[12] A. J. Schellekens and B. Koopmans, Phys. Rev. B **87**, 020407 (2013).
[13] C. Boeglin, E. Beaurepaire, V. Halté, V. López-Flores, C. Stamm, N. Pontius, H. Dürr, and J.-Y. Bigot, Nature (London) **465**, 458 (2010).
[14] C. Graves, A. Reid, T. Wang, B. Wu, S. de Jong, K. Vahaplar, I. Radu, D. Bernstein, M. Messerschmidt, L. Müller *et al.*, Nat. Mater. **12**, 293 (2013).
[15] B. Vodungbo, J. Gautier, G. Lambert, A. B. Sardinha, M. Lozano, S. Sebban, M. Ducousso, W. Boutu, K. Li, B. Tudu *et al.*, Nat. Commun. **3**, 999 (2012).
[16] I. Radu, G. Woltersdorf, M. Kiessling, A. Melnikov, U. Bovensiepen, J.-U. Thiele, and C. H. Back, Phys. Rev. Lett. **102**, 117201 (2009).
[17] I. Radu, K. Vahar, C. Stamm, T. Kachel, N. Pontius, H. Dürr, T. Ostler, J. Barker, R. Evans, R. Chantrell *et al.*, Nature (London) **472**, 205 (2011).
[18] S. Mangin, M. Gottwald, C. Lambert, D. Steil, V. Uhlíř, L. Pang, M. Hehn, S. Alebrand, M. Cinchetti, G. Malinowski *et al.*, Nat. Mater. **13**, 286 (2014).
[19] A. Eschenlohr, Ph.D. thesis, Universität Potsdam, 2012.
[20] S. Mathias, L.-O. Chan, P. Grychtol, P. Granitzka, E. Turgut, J. M. Shaw, R. Adam, H. T. Nembach, M. E. Siemens, S. Eich *et al.*, Proc. Natl. Acad. Sci. USA **109**, 4792 (2012).
[21] B. Y. Mueller, A. Baral, S. Vollmar, M. Cinchetti, M. Aeschlimann, H. C. Schneider, and B. Rethfeld, Phys. Rev. Lett. **111**, 167204 (2013).
[22] L. M. Sandratskii and P. Mavropoulos, Phys. Rev. B **83**, 174408 (2011).
[23] I. Radu, C. Stamm, N. Pontius, T. Kachel, P. Ramm, J.-U. Thiele, H. A. Dürr, and C. H. Back, Phys. Rev. B **81**, 104415 (2010).
[24] C. Grazioli, C. Callegari, A. Ciavardini, M. Coreno, F. Frassetto, D. Gauthier, D. Golob, R. Ivanov, A. Kivimäki, B. Mahieu, B. Bučar, M. Merhar, P. Miotti, L. Poletto, E. Polo, B. Ressel, C. Spezzani, and G. De Ninno, Rev. Sci. Instrum. **85**, 023104 (2014).
[25] X. F. Li, A. L'Huillier, M. Ferray, L. A. Lompré, and G. Mainfray, Phys. Rev. A **39**, 5751 (1989).
[26] Z. Chang, A. Rundquist, H. Wang, M. M. Murnane, and H. C. Kapteyn, Phys. Rev. Lett. **79**, 2967 (1997).
[27] L. Poletto and F. Frassetto, Appl. Opt. **49**, 5465 (2010).
[28] L. Poletto and F. Frassetto, Appl. Sci. **3**, 1 (2013).
[29] M. Sacchi, C. Spezzani, P. Torelli, A. Avila, R. Delaunay, and C. F. Hague, Rev. Sci. Instrum. **74**, 2791 (2003).
[30] C. La-O-Vorakiat, M. Siemens, M. M. Murnane, H. C. Kapteyn, S. Mathias, M. Aeschlimann, P. Grychtol, R. Adam, C. M. Schneider, J. M. Shaw, H. Nembach, and T. J. Silva, Phys. Rev. Lett. **103**, 257402 (2009).
[31] S. Valencia, A. Gaupp, W. Gudat, H.-C. Mertins, P. Oppeneer, D. Abramsohn, and C. Schneider, New J. Phys. **8**, 254 (2006).
[32] See Supplemental Material at http://link.aps.org/supplemental/10.1103/PhysRevB.90.180407 for a detailed description of the data treatment and fitting procedure.
[33] C. Stamm, J.-U. Thiele, T. Kachel, I. Radu, P. Ramm, M. Kosuth, J. Minár, H. Ebert, H. A. Dürr, W. Eberhardt, and C. H. Back, Phys. Rev. B **77**, 184401 (2008).
[34] C. Bordel, J. Juraszek, D. W. Cooke, C. Baldasseroni, S. Mankovsky, J. Minár, H. Ebert, S. Moyerman, E. E. Fullerton, and F. Hellman, Phys. Rev. Lett. **109**, 117201 (2012).
[35] C. Illg, M. Haag, and M. Fähnle, Phys. Rev. B **88**, 214404 (2013).
[36] D. W. Cooke, F. Hellman, C. Baldasseroni, C. Bordel, S. Moyerman, and E. E. Fullerton, Phys. Rev. Lett. **109**, 255901 (2012).
[37] A. J. Schellekens and B. Koopmans, Phys. Rev. Lett. **110**, 217204 (2013).
[38] J. Hohlfeld, S.-S. Wellershoff, J. Güdde, U. Conrad, V. Jähnke, and E. Matthias, Chem. Phys. **251**, 237 (2000).
[39] J. Güdde, J. Hohlfeld, J. Müller, and E. Matthias, Appl. Surf. Sci. **127-129**, 40 (1998).
[40] Z. Lin, L. V. Zhigilei, and V. Celli, Phys. Rev. B **77**, 075133 (2008).